# Development of a Model Output Statistic and implementation of an operational solar photovoltaic energy forecast model based in WRF

Claudio Porrini , Alejandro Gutiérrez and Gabriel Cazes Boezio
IMFIA, Facultad de Ingeniería de la Universidad de la República, *Montevideo Uruguay.*

Gonzalo Hermida, Diego Oroño and Martin Puppo
IIE, Facultad de Ingeniería de la Universidad de la República, *Montevideo Uruguay.*

***Abstract*—In this work, an operational solar energy forecast model was developed based in correction of irradatiation obtained from WRF output. This output depends on the Hourly Clearness Index (kt). Three different physic schemes of WRF parametrization are analyzed in this work. The horizontal irradiation computed by Weather Research and Forecasting (WRF) is the input of the developed Model Output Statistic (MOS). Solar irradiation is converted from horizontal to tilted surface, and a final photo-voltaic solar energy plant coefficient is calibrated to obtain the minimal absolute error in the period of calibration.**

***Index Terms*—solar energy, forecast.**

## I. Introduction

Uruguay is changing its energetic matrix by introducing non conventional renawable energy sources, such as wind and solar power, aiming to 1718.2 MW by the year 2016. The solar power capacity to be installed in the country will be 236.7 MW [1]. This means that the system will reach a penetration factor into the electrical system of 5%. This factor is defined as the ratio of photovoltaic and total power capacity. In order to improve experience in research and introducing solar power into the Uruguayan electric grid, a photo-voltaic (PV) plant was installed in the north of the country, region were irradiation reaches its maximum values.

The solar irradiation data used in this work was provided by the national electric utility of Uruguay (UTE). In this work, a Model Output Statistic based in WRF simulations for three different physics schemes will be presented. First of all, the horizontal solar irradiation MOS-WRF model will be presented. Conversion from horizontal to tilted surface is computed, then the solar plant MOS model is calibrated and implemented in an operational forecast model.

## II. Measured Solar Irradiance and Pv-Solar Plant

This work analyzes observational data recorded by the National Electric Company of Uruguay (UTE), and historical data of the solar photovoltaic plant UTE-ASHAI. Solar irradiance measurements are made with Li-Cor LI-200SZ model NRG Pyranometers, sampled at a rate of 2 seconds. An installed commercial data logger registered the mean, maximun and standard deviation every 10 minutes. For this work, hourly data is computed and used for the analysis. Pyranometer measurements and ASHAI solar plant locations are presented in Fig. 1. In table 1, geographical locations and stations codes are presented.

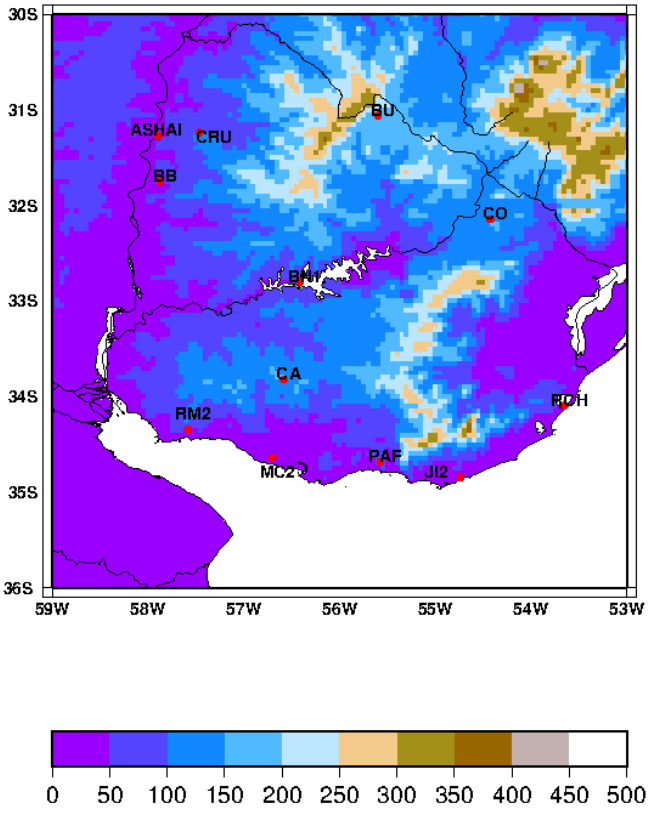


Fig.1. Pyranometer measurements, ASHAI solar plant location, and uruguayan topography expressed in meters.

| STATION | CODE | LAT | LON |
|---|---|---|---|
| Jose Ignacio | JI2 | -34.682 | -55.575 |
| Rosendo Mendoza | RM2 | -34.343 | -57.578 |
| Rocha | RCH | -34.094 | -53.65 |
| Colonia Otamendi | CO | -32.142 | -54.422 |
| Colonia Arias | CA | -33.823 | -56.583 |
| Piedras de Afilar | PAF | -34.682 | -55.575 |
| McMeekan | MC2 | -34.643 | -56.695 |
| Buena Unión | BU | -31.059 | -55.602 |
| Bonete | BN1 | -32.8 | -56.415 |
| Colonia Rubio | CRU | -31.238 | -57.465 |
| Baltazar Brum | BB | -31.78 | -57.868 |

Table 1. Stations and geographical location.

*A. WRF simulations*

The radiation schemes provide atmospheric heating due to radiative flux divergence and surface downward long-wave and short-wave radiation for the ground heat budget. The only source is the Sun, but processes include absorption, reflection, and scattering in the atmosphere and at surfaces. All the radiation schemes in WRF are column (one-dimensional) schemes, so each column is treated independently [3]. The simulations use initial and boundary conditions in a bigger domain, provided by the Global Forecast System (GFS) of the National Oceanic and Atmospheric Administration (NOAA) National Weather Service NCEP, downloaded from NOAA. Initial and boundary conditions are provided by the NOAA GFS at 00:00, 06:00, 12:00 and 18:00 GMT. The WRF run uses time horizon from 0 to 6 hours, with grid nudging. In Table 2 is presented the physics schemes that was run to develop the forecast of the irradiation in horizontal plane. Year 2012 was used in this work.

| Physics Schemes | 1 | 2 | 3 |
|---|---|---|---|
| **Microphysics** | Lin(Purdue) [2] | Lin(Purdue) [2] | WSM3 [3] |
| **Cumulus Parametrization** | Kain-Fritsch scheme [4] | Kain-Fritsch scheme [4] | Kain-Fritsch scheme [4] |
| **Land-Surface Model** | Noah [5] | Noah [5] | Noah [5] |
| **Planetary Boundary Layer** | MYJ [6] | MYJ [6] | YSU [7] |
| **Atmospheric Radiation** | CAM scheme [8] | rrtmg scheme [9] | Dudhia Scheme [10] |

Table 2. Physical schemes applied in the evaluation of the solar energy forecast model for the photo-voltaic solar plant.

In each configuration of WRF, two domains are nested when running. The first domain has an horizontal resolution of 30 km and the second one, high resolution domain, is 10 km. This domain covers all pyranometer measurements which are used for calibration and cross validation. Fig. 2 shows the grid domain used in the simulations.

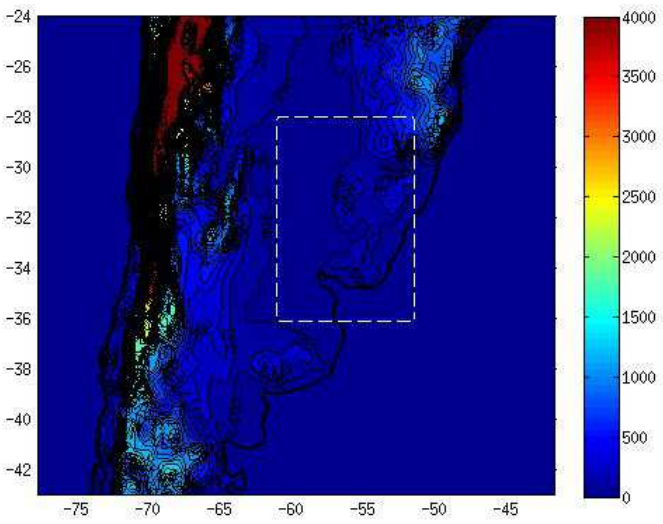


Fig.2. Domain d01 30 km grid resolution, and high resolution domain 10 km, topography plotted.

*B. Horizontal irradiation Model Output Statistic*

The Model Output Statistics (MOS) considers the historical data of solar irradiation measured with the observational pyranometer network of UTE, and computed horizontal irradiation by WRF model for different physical schemes. The MOS was calibrated with irradiation data from five stations distributed along the country. Year 2012 data was used in this work.

The MOS correction uses the WRF output, and is also based on the Clearness Index Kt. This index is defined in Eq.1 as the ratio of the horizontal global irradiation I to the corresponding irradiation available on the top of the atmosphere I0 in an hourly basis.

$$kt = I/I_o \quad (1)$$

Three different atmospheric conditions are defined in the MOS model for the correction of WRF output:

$kt < 0.4$ cloudy conditions
$0.4 \leq kt < 0.65$ partially cloudy conditions
$kt \geq 0.65$ clear sky conditions

The MOS is calibrated with a linear regression approach. In order to obtain the best fit for irradiation forecast computing, a coefficient is adjusted using the three WRF

irradiation schemes and the observed irradiation. $I_{OBS}^{kt}$ is the irradiation observed during the period of calibration in the kt condition previously defined, and $I_{WRF}^{kt}$ is the computed irradiation by WRF simulation. Therefore, the calibration coeffcient $\rho(kt)$ is computed for different conditions of kt, according to Eq. 2.

$$I_{OBS}^{kt}=\rho(kt)I_{WRF}^{kt} \quad (2)$$

Five stations were chosen as the training group for the calibration of MOS-WRF model. These were: BO, BU, BB, RCH and RM. A map of coefficients was constructed by interpolation for all regions of the country.

The coefficients $\rho(kt)$ for six stations that result for the interpolation computed in the calibration process are presented in table 3.

| SCHEME 1 | kt < 0,4 | 0,4 ≤ kt <0,65 | kt ≥ 0,65 |
|---|---|---|---|
| CR | 0,40 | 0,77 | 0,98 |
| CA | 0,33 | 0,80 | 0,96 |
| CO | 0,37 | 0,85 | 1,01 |
| JI | 0,37 | 0,81 | 0,98 |
| MC | 0,38 | 0,80 | 0,98 |
| PA | 0,34 | 0,81 | 0,97 |
| **SCHEME 2** | **kt < 0,4** | **0,4 ≤ kt <0,65** | **kt ≥ 0,65** |
| CR | 0,37 | 0,76 | 0,98 |
| CA | 0,32 | 0,80 | 0,96 |
| CO | 0,35 | 0,81 | 0,99 |
| JI | 0,35 | 0,79 | 0,97 |
| MC | 0,35 | 0,79 | 0,98 |
| PA | 0,33 | 0,80 | 0,96 |
| **SCHEME 3** | **kt < 0,4** | **0,4 ≤ kt <0,65** | **kt ≥ 0,65** |
| CR | 0,38 | 0,72 | 0,99 |
| CA | 0,34 | 0,75 | 0,98 |
| CO | 0,37 | 0,75 | 1,00 |
| JI | 0,35 | 0,74 | 0,99 |
| MC | 0,36 | 0,73 | 0,99 |
| PA | 0,34 | 0,75 | 0,96 |

Table 3. Calculated coefficients for different locations in Uruguay for each kt classification. These coefficients were obtained from an interpolated map constructed with the training group.

For the same six stations, the MAE and RMSD are computed as statistical model indicators. Results are presented in Table 4 for the three differents schemes, showing that the raw WRF irradiation output is overestimated for each kt classification in an hourly basis. For cloudy conditions, large errors were found, in an order of more than 100 % in rMAE for each radiation scheme. In some cases, an rMAE error of 146 % was found. Better results are obtained for partially cloudy conditions, but the errors obtained are still large. In the case of clear sky conditions, irradation obtained from WRF raw output is well represented in the majority of the simulated cases. Nevertheless, also improvements were found for clear sky conditions MOS-WRF.

Once MOS technique is used, results improve dramatically for non-clear conditions, leading to lower rMAE errors down to half than those encountered with WRF raw output. The best results were found for the CAM scheme.

| SCHEME 1 | | WRF RAW | | MOS-WRF | |
|---|---|---|---|---|---|
| | | rMAE | rRMSD | rMAE | rRMSD |
| kt < 0,4 | CR | 145 | 208 | **55** | **75** |
| | CA | 127 | 190 | **52** | **72** |
| | CO | 131 | 188 | **56** | **75** |
| | JI | 109 | 162 | **52** | **70** |
| | MC | 119 | 180 | **55** | **76** |
| | PA | 119 | 175 | **49** | **67** |
| 0,4≤kt<0,65 | CR | 46 | 55 | **26** | **35** |
| | CA | 44 | 56 | **28** | **38** |
| | CO | 47 | 56 | **31** | **40** |
| | JI | 38 | 50 | **30** | **41** |
| | MC | 43 | 55 | **28** | **38** |
| | PA | 42 | 54 | **29** | **38** |
| kt≥0,65 | CR | 19 | 23 | **16** | **21** |
| | CA | 15 | 22 | **13** | **22** |
| | CO | 22 | 28 | **20** | **27** |
| | JI | 15 | 22 | **15** | **22** |
| | MC | 15 | 21 | **13** | **21** |
| | PA | 15 | 20 | **14** | **20** |
| **SCHEME 2** | | **WRF RAW** | | **MOS-WRF** | |
| | | **rMAE** | **rRMSD** | **rMAE** | **rRMSD** |
| kt < 0,4 | | 171 | 229 | **51** | **67** |
| | | 145 | 204 | **47** | **65** |
| | | 145 | 196 | **51** | **68** |
| | | 139 | 190 | **46** | **63** |

| | | | | |
|---|---|---|---|---|
| | 154 | 212 | **65** | **47** |
| | 155 | 207 | **44** | **61** |
| **0,4≤kt<0,65** | 44 | 52 | **21** | **28** |
| | 42 | 54 | **21** | **30** |
| | 43 | 53 | **23** | **30** |
| | 41 | 53 | **24** | **33** |
| | 43 | 54 | **20** | **28** |
| | 43 | 56 | **22** | **30** |
| **kt≥0,65** | 14 | 17 | **11** | **14** |
| | 9 | 14 | **8** | **13** |
| | 15 | 19 | **11** | **15** |
| | 10 | 16 | **10** | **16** |
| | 10 | 14 | **8** | **14** |
| | 11 | 14 | **9** | **12** |
| **SCHEME** 3 | WRF RAW | | **MOS-WRF** | |
| | **rMAE** | **rRMSD** | **rMAE** | **rRMSD** |
| **kt < 0,4** | 146 | 211 | **54** | **73** |
| | 123 | 188 | **60** | **82** |
| | 122 | 190 | **62** | **86** |
| | 115 | 174 | **57** | **77** |
| | 122 | 190 | **62** | **84** |
| | 125 | 189 | **57** | **79** |
| **0,4≤kt<0,65** | 43 | 52 | **23** | **32** |
| | 44 | 56 | **33** | **46** |
| | 43 | 54 | **31** | **43** |
| | 44 | 55 | **33** | **46** |
| | 42 | 54 | **31** | **43** |
| | 44 | 55 | **32** | **44** |
| **kt≥0,65** | 19 | 25 | **18** | **24** |
| | 18 | 27 | **17** | **27** |
| | 15 | 24 | **15** | **24** |
| | 18 | 27 | **18** | **27** |
| | 15 | 24 | **15** | **24** |
| | 16 | 25 | **15** | **24** |

Table 4. rMAE and rRMSD results for each station used for validation of the model.

### *C. Solar irradiation conversion from horizontal to tilted surface*

Incident solar irradiation on a surface depends on its position. Once the surface position is defined, and knowing the relative position of the sun, the incidence angle (between the Sun-Earth line and the surface's normal) may be determined using Eq. 3 [13],

$$\cos\theta = [(\sin\delta\cos\phi - \cos\delta\sin\phi\cos\omega)\cos\gamma + \cos\delta\sin\omega\sin\gamma]\sin\beta + [\sin\delta\sin\phi + \cos\delta\cos\phi\cos\omega]\cos\beta \quad (3)$$

where, $\delta$ is solar declination, $\omega$ is the hourly angle, $\phi$ corresponds to the latitude where the surface is located, $\gamma$ is the azimuth (angle between the surface's normal projection on the horizontal plane and the observer's meridian) and $\beta$ the tilt of the surface.

Global irradiation Ii on a tilted surface can be calculated from horizontal measures and depends on cosθ. Global irradiation can be calculated as the sum of three components, according to Eq. 4.

$$I_i = I_{bi} + I_{di} + I_{ri} \quad (4)$$

where $I_{bi}$ is the Direct Irradiation, $I_{di}$ is the Diffuse Irradiation and $I_{ri}$ is the Reflected Irradiation.

Direct irradiation is the one that comes directly from the Sun. Therefore, its direction is collinear to the Earth-Sun line. This component is predominant in the global irradiation. To calculate it, the direct ratio is defined, as the ratio between the hourly direct irradiation on an inclined surface and a horizontal one.

$$r_{bi} = \frac{I_{bi}}{Ibh} = \frac{I_{bn}\cos\theta}{I_{bn}\cos\theta_z} = \frac{\cos\theta}{\cos\theta_z} \quad (5)$$

The second component is the diffuse irradiation. This type of irradiation isn't totally isotropic. While the largest proportion of it's total is actually isotropic (Isotropic Component), the diffuse irradiation exhibits an increase of intensity in the Earth-Sun direction (surrounding the Sun). This contribution is named "Circumsolar Irradiation". On clear days, the sky tends to be brighter near the horizon. This phenomena is called "Horizon Brightness", and is another of the contributing components of the diffuse irradiation.

Several models that represent diffuse irradiation coexist. In the current work, the HDKR (Hay, Davies, Klucher y Reindl) [13] was implemented in the model. This model is explicit in Eq. 6, and it considers all of the three mentioned components: isotropic, circumsolar, horizon brightness.

$$I_{di}=I\_dh[(1-T_b)(\frac{1+\cos\beta}{2})(1+\sqrt{1-f_d}\left(\sin\frac{\beta}{2}\right)^3+T_b r_b \quad (6)$$

where the term $\frac{1+\cos\beta}{2}$ is the view factor (with which the surface "sees" the sky), and the term $I_{dh}$ is the diffuse irradiation value on a horizontal surface. Also, atmospheric transmittance $T_b$ is used as an anisotropic indicator. This factor is calculated as the ratio between the direct and extraterrestrial irradiation as in Eq. 7,

$$T_b=\frac{I_{bn}}{I_{on}}=\frac{I_{bh}}{I_{oh}}=(1-f_d)kt \quad (7)$$

The parameter $f_d$ is defined as the proportion of diffuse reflected irradiation in relation to global irradiation in Eq. 8.

$$f_d=\frac{I_{dh}}{I_{gh}} \quad (8)$$

Finally, the diffused reflected irradiation that depends on the reflectance coefficients of the surface is and is given by Eq. 9,

$$I_{ri}=\frac{(1+\cos\theta)}{2} I_h \quad (9)$$

In order to be able to calculate the expression before, it is necessary to isolate direct and diffuse irradiation, because the model processes them differently. To separate the different components that make global irradiation, empirical correlations or physical models must be used. Several correlation have been created for this purpose. In this work, the correlation presented in [14] is used.

### *D. Photovoltaic plant model*

The photovoltaic plant is composed by 215 Wp Sanyo HIT solar panels, with a total power of 0.50 MW. HIT is an hybrid solar cell, composed of a single-crystal silicon wafer surrounded by layers of thin amorphous silicon.

A power forecasting model was developed for the photovoltaic plant. This model attempts to estimate the energy that will be generated and introduced to the electric grid. The calibration period for this model was during the warmest season of the southern hemisphere, from October 2013 to March 2014.

The main input parameters for the development of this forecast PV model are the irradiation product obtained from the MOS-WRF, explained before in the previous section, and the historical data of the ASAHI PV plant. These two parameters allow to construct a calibrated model for the plant of interest.

A schematic summary of the model development is illustrated in figure 3.

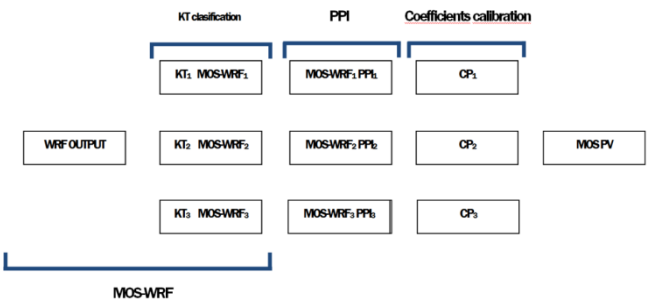


Figure 3. Schematic flow chart of photovoltaic model concepts.

Three important steps were made and are described next:

*1) MOS-WRF irradiation data as input.*

MOS-WRF irradiation on horizontal surface data is generated by the model described before and is dependent on atmospheric conditions given by the mentioned hourly index clearness classification. As a consequence, the photovoltaic forecasting model plant will be also dependent on *kt* index.

*2) Passage from irradiation on horizontal plane to irradiation on tilted surface (PPI).*

Passage from horizontal to tilted surface must be done in order to find the best coefficients that adjust to the observational data of the photovoltaic plant. This passage can be done applying HDKR model with the Arias correlation explained in section C.

*3) Calibration of coefficients for photovoltaic plant model.*

A fine calibration of the model is required in order to obtain reasonable energy predictions from the irradiation forecast data.

For this reason, the coefficients are estimated with the same MOS technical approach described in B. In this case, the computed coefficients consider the global irradiation in tilted surface and the power data of ASAHI photovoltaic plant. This fitting was made according to Eq. 10,

$$PV^{kt}_{WRF,PPI}=c_{PV}(kt)\, I^{kt}_{WRF,PPI} \quad (10)$$

where $I^{kt}_{WRF,PPI}$ is the irradation in tilted surface obtained form MOS-WRF and the passage from horizontal to tilted surface, $c_{PV}(kt)\, I^{kt}_{WRF,PPI}$ is the fitted coefficient and $PV^{kt}_{WRF,PPI}$ is the measured data of the photovoltaic plant. Each of this parameters depend on the index clearness classification made before, so three coefficients are found as a result of this calibration, as seen in table 5.

| | Clear Sky | Partial Cloudy | Cloudy |
|---|---|---|---|
| $cp_{PV}(MW(W/m^2)^{-1})$ | 0.00036 | 0.00027 | 0.00025 |

Table 5. Calibration coefficient for forecast model PV plant. For each atmospheric condition.

### *E. Results and discussions*

Model's performance can be seen by observing the error histogram shown in figure 4. This histogram was calculated as the difference between the measured power and the model forecast power. Forecast power is well represented by the developed model. Almost 70 % of forecast cases are in the error band of ± 0.05 MW. The Mean Absolute Error represents an error of 5 % respect to the maximum power generated by the 0.50 MW photovoltaic plant. The histogram was computed for a period with a significant number of clear sky condition hours.

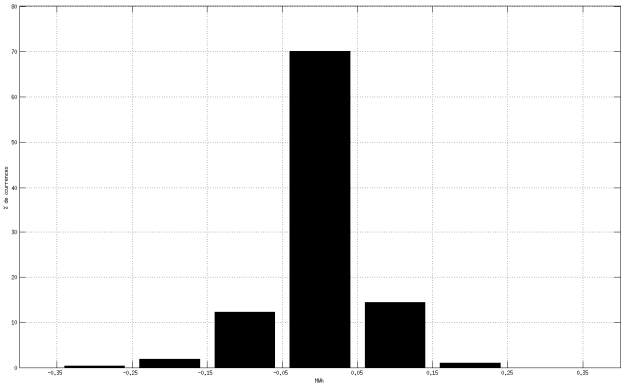

Figure 4. Error histogram of solar forecasting for PV plant ASAHI. Error histogram is constructed as the difference of observed power minus forecast power.

## III. CONCLUSIONS

WRF irradiation output is overestimated for each kt classification in an hourly basis. For cloudy conditions it was found that error were significantly larger in comparison to clear sky conditions, in an order of more than 100% in rMAE for each radiation scheme used for each simulation. In some particular cases, an rMAE error of 146% was found. For partially cloudy conditions resutls obtained are better, but the errors found are still large. For clear sky conditions, irradation obtained from WRF raw output is well represented in the majority of the simulated cases. When the MOS technique was used, results improved dramatically for cloudy and partially cloudy conditions, leading to lower the rMAE error down to half than those encountered with WRF raw output. Improvements for clear sky conditions were also found. Of the three studied cases, the CAM scheme was found to be the most accurate. The results shown in this study conclude that the developed photovoltaic power forecasting model leads to good representation of the ground truth behavior of the plant.

In future works, the model will be analyzed for a longer period of time and with other solar plants' data, leading to a more robust validation.


## ACKNOWLEDGMENT

The present results are from the ANII FSE_1_2013_1_10975 “Aplicación de herramientas de HPC, para el desarrollo de un sistema de pronóstico operativo de la generación de energía eléctrica de plantas fotovoltaicas” project development and recent advances of an agreement for implementation of a forecast system of wind energy power input to the national grid between the Administración Nacional de Usinas y Trasmisiones Eléctricas (UTE), and the School of Engineering UdelaR.


## REFERENCES


[1] Uruguay XXI, Energías Renovables, Agosto 2014.

[2] Skamarock, 2008 NCAR/TN 475+STRNCAR TECHNICAL NOTE June 2008 A Description of the Advanced Research WRF Version 3

[3] Lin, Yuh–Lang, Richard D. Farley, and Harold D. Orville, 1983: Bulk Parameterization of the Snow Field in a Cloud Model. *J.Climate Appl. Met.*,**22**, 1065–1092.

[4] Hong, Song–You, Jimy Dudhia, and Shu–Hua Chen, 2004: A revised approach to ice microphysical processes for the bulk parameterization of clouds and precipitation. , 132, 103–120.

[5] Kain, John S., 2004: The Kain–Fritsch convective parameterization: An update. *J. Appl. Meteor.*, **43**, 170–181

[6] Tewari, M., F. Chen, W. Wang, J. Dudhia, M. A. LeMone, K. Mitchell, M. Ek, G. Gayno, J. Wegiel, and R. H. Cuenca, 2004: Implementation and verification of the unified NOAH land surface model in the WRF model. *20th conference on weather analysis and forecasting/16th conference on numerical weather prediction*, pp. 11–15.

[7] Janjic, Zavisa I., 1994: The Step–Mountain Eta Coordinate Model: Further developments of the convection, viscous sublayer, and turbulence closure schemes. *Mon. Wea. Rev.*,**122**, 927–945.

[8] Hong, Song–You, Yign Noh, Jimy Dudhia, 2006: A new vertical diffusion package with an explicit treatment of entrainment processes. Mon. Wea. Rev., 134, 2318–2341.

[9] Collins, William D., et al., 2004: Description of the NCAR Community Atmosphere Model (CAM 3.0). NCAR Tech. Note NCAR/TN–464+STR. 214 pp.

[10] Iacono, M. J., J. S. Delamere, E. J. Mlawer, M. W. Shephard, S. A. Clough, and W. D. Collins, 2008: Radiative forcing by long–lived greenhouse gases: Calculations with the AER radiative transfer models. J. Geophys. Res., 113, D13103.

[11] Dudhia, J., 1989: Numerical study of convection observed during the Winter Monsoon Experiment using a mesoscale two–dimensional model. *J. Atmos. Sci.*, **46**, 3077–3107.

[12] Course Notes: Solar Energy Fundamentals. Gonzalo Abal, Institute of Physics, Faculty of Engineering, UdelaR

[13] Solar Engineering of Thermal Processes. John A. Duffie, William A. Beckman. Wiley and Sons, Hoboken, New Jersey, third edition, 2006.

[14] Proposal of a Regressive Model for the Hourly Diffuse Solar Radiation Under All Sky Conditions. J.A Ruiz-Arias, H. Alsamamra, J. Tovar-Pescador, D. Pozo-Vázquez, Energy Con-version and Management 2010.